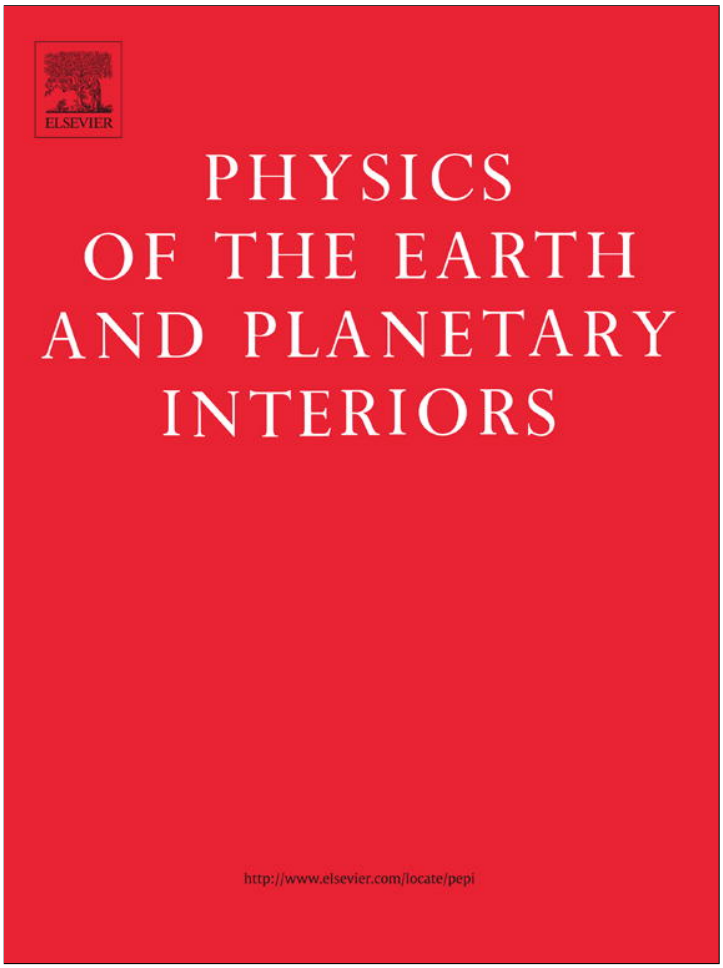

(This is a sample cover image for this issue. The actual cover is not yet available at this time.)

Physics of the Earth and Planetary Interiors 206-207 (2012) 67–75

Contents lists available at SciVerse ScienceDirect

Physics of the Earth and Planetary Interiors

journal homepage: www.elsevier.com/locate/pepi

Geodetic strain rate and earthquake size: New clues for seismic hazard studies

Federica Riguzzi [a,*], Mattia Crespi [b], Roberto Devoti [a], Carlo Doglioni [c], Grazia Pietrantonio [a], Anna Rita Pisani [a]

[a] Istituto Nazionale di Geofisica e Vulcanologia, sez. CNT, Roma, Italy
[b] Area di Geodesia e Geomatica -DICEA, Università di Roma La Sapienza, Roma, Italy
[c] Dipartimento di Scienze della Terra, Università di Roma La Sapienza, Roma, Italy

ARTICLE INFO

Article history:
Received 19 March 2012
Received in revised form 5 July 2012
Accepted 12 July 2012
Available online 26 July 2012
Edited by Mark Jellinek

Keywords:
Strain rate
Magnitude
Gutenberg–Richter law
Bayesian analysis
Seismic hazard
Italian area
L' Aquila
Emilia earthquakes

ABSTRACT

Earthquakes deliver in few seconds the elastic energy accumulated in hundreds of years. Where and when will be the next earthquake remains a difficult task due to the chaotic behaviour of seismicity and the present lack of available tools to measure the threshold of the crustal strength.

However, the analysis of the background strain rate in Italy and the comparison with seismicity shows that larger earthquakes occur with higher probability in areas of lower strain rate. We present a statistical study in which a relationship linking the earthquake size (magnitude) and the total strain rate (SR) is found. We combine the information provided by the Gutenberg–Richter law (GR) of earthquake occurrence and the probability density distribution of SR in the Italian area. Following a Bayesian approach, we found a simple family of exponential decrease curves describing the probability that an event of a given size occurs within a given class of SR. This approach relies on the evidence that elastic energy accumulates in those areas where faults are locked and the SR is lower. Therefore, in tectonically active areas, SR lows are more prone to release larger amount of energy with respect to adjacent zones characterised by higher strain rates. The SR map of Italy, compared with 5 years seismicity supports this result and may become a powerful tool for identifying the areas more prone to the next earthquakes.

1. Introduction

Earthquake hazard analyses strongly depend on how the spatial distribution of earthquakes is interpreted: are seismic gaps areas of high hazard waiting to be filled by new earthquakes, or are the gaps aseismic and thus represent zones of low hazard? This two-fold view derives from considering sometimes short-term and some other times long-term processes (e.g., Stein, 1992). The interpretation of crustal deformation mainly depends on the timescale of the modelled processes, the crust deforms elastically over short periods, permanently when the stresses exceed the yield strength (coseismic deformation) and viscously over long geological time scales. The resultant crustal evolution is differently recorded by GPS networks and geologically derived deformation rates. GPS measures the displacements within the earthquake cycle, but due to the viscoelastic behaviour of the crust, the deformation differs significantly early and late in the cycle. Early in the cycle, viscous flow in the lower crust exerts a traction on the upper crust and produces high velocity gradients near the fault. Late in the cycle the opposite occurs and the velocity gradients decrease near the faults (e.g., Savage and Prescott, 1978; Dixon et al., 2002; Lundgren et al., 2009).

Velocity gradients, in particular the strain rate components, and variations of the interplate coupling are the major outcomes of GPS networks playing an important role in assessing the seismic hazard in active tectonic areas (e.g., Loveless and Meade, 2011). Some approaches follow a time dependent analysis in which two critical items in the energetic budget of seismic areas are the strain rate, which is measured geodetically on the Earth's surface, and the yearly number of earthquakes exceeding a given magnitude (e.g., Caporali et al., 2011). At global scale, the correlation found between seismicity rates and tectonic moment rates (Kreemer et al., 2003; Bird et al., 2010) for subduction zones and regions of continental deformation supports their use as an indicator of tectonic activity and hazard. At local scale, other approaches rely on the systematic determination of fault slip rates at geological (late Pleistocene–Holocene) and geodetic (decadal) time scales. The analysis of both long-term and short-term fault behaviours is also important for understanding stress loading and slip processes throughout successive seismic cycles, providing insights into seismic hazard (e.g., Fialko, 2006; Cavalié et al., 2008).

Areas of aseismic gap (or areas of low seismicity) may be either zones where faults are creeping in a steady-state regime, and no elastic strain is accumulated, or areas where the faults are locked

* Corresponding author.
E-mail address: federica.riguzzi@ingv.it (F. Riguzzi).

0031-9201/$ - see front matter © 2012 Elsevier B.V. All rights reserved.
http://dx.doi.org/10.1016/j.pepi.2012.07.005

and loading higher amount of elastic strain. On the other hand, it has been shown that some areas with high strain rates undergo on average to high seismic activity (Shen et al., 2007); but to evaluate the hazard of such areas one has to know whether the seismic cycle is in an early or later phase. High strain rates in certain regions may result from, rather than precede an earthquake (Hammond et al., 2010).

Recently, the geodetic strain rate mapping prior to seismic events in extensional, contractional and strike-slip tectonic settings has evidenced how earthquakes are generated along fault segments with lower strain rate with respect to neighbouring higher strain rate areas (Doglioni et al., 2011). Thus, strain rate mapping from interseismic GPS velocities may constitute an indicator of future seismic event occurrence. Therefore we treat the regional SR as a stochastic variable, studying the correlation between the seismicity and local deformation; under this hypothesis, we show that the probability that an event of a given magnitude may occur within a given class of SR can be described through a simple family of exponential decrease curves.

This statistical approach, associated to an accurate mapping of the present SR and usefully combined with classical hazard studies, e.g., mapping of active faults based on geological evidences, historical seismicity, GPS velocity gradients, and rheological studies constrained by the heat flow map of a given region, could represent a new tool in order to determine the areas where the higher seismic risk is concentrated in tectonically active regions.

2. Strain rate map of Italy

The Apennines are generated by the westerly directed subduction of the Adriatic plate (e.g., Doglioni, 1991), whereas in the Alps the European plate is subducting underneath the Adriatic plate (Dal Piaz, 2010), as schematically shown in Fig. 1A. Both subduction zones experience seismicity, which is more pronounced along the ridge of the Apennines, and in the foothills of the Alps. The Apennines subduction is characterised by compressional seismicity east of the chain, in the frontal accretionary prism, and extensional tectonics to the west, associated to the opening of the Tyrrhenian backarc basin. The whole area presently undergoes about 5–10 mm/yr differential motion either in convergent, extension and transfer tectonic settings, depending on the behaviour of the subduction hinge (Devoti et al., 2008).

In this work the strain rate tensor estimation is based on the recent GPS velocity solution of the Italian area provided by Devoti et al. (2011) and shown in Fig. 2 of the same paper. The rates of 298 GPS sites have been estimated simultaneously in a least-squares inversion of all the daily coordinate and covariance solutions stacked to form the normal equations, according to the following functional model

$$x_i(t) = x_i^0 + r_i \cdot t + \alpha_i \cdot \sin(\omega t + \varphi_i) + \Delta x_i \cdot \sum_j H(t_j)$$

where x_i are the Cartesian coordinates of each site ($i = 1, 2, 3$), x_i^0 is the constant and r_i the rate of the fitting straight line, α and φ are, respectively the amplitude and phase of annual signals ($\omega = 2\pi f$, f being the annual frequency) and H is the Heaviside step-function used to model eventual coordinate offsets (Δx_i) at a given time t_j. The rates r_i estimated by the linear model represent the interseismic velocities during the seismic cycle (e.g., Liu et al., 2000). For those sites affected by coseismic (Anzidei et al., 2009) and postseismic deformations (e.g., Devoti et al., in press) as a consequence of the L'Aquila earthquake (6 April 2009, Mw 6.3, M_L 5.9), we have limited the interseismic velocities estimation up to the day before the earthquake epoch. We have estimated the GPS velocities from 2.5 to ~11 years of position determinations, thus minimizing biases due to seasonal signals (Blewitt and Lavallée, 2002). To avoid spurious strain rate features, isolated velocity vectors that differ significantly from their next neighbours have been rejected as outliers. The maximum effort in deploying the GPS networks in Italy dates back to about 2005 (Avallone et al., 2010), so that we consider the contribution of the velocity field to the interseismic strain rate estimation effective since about 2007.

The 2D strain rate tensor has been evaluated from the horizontal GPS velocities and the associated uncertainties by a distance-weighted approach obtained using all stations on a regularly spaced grid and applying the weighting algorithm developed by Shen et al. (1996). The contribution of each station velocity to the strain rate computed on a given node is down weighted with the function $W = \exp(-d^2/\alpha^2)$, where d is the distance between each node and the stations and α defines the effective geographic width of the smoothing kernel. The algorithm selects the optimal α-value from a given a priori interval, depending on the spatial distribution of the GPS sites, consequently strain rate maps are obtained with spatially variable α. Stations located within 1α distance contribute more than 37% to the least squares inversion, whereas those at distance greater than 2α contribute less than 2% (Shen et al., 2007). This approach necessarily produces a smoothing of patterns, making it difficult to relate steep strain gradients to individual structures, nevertheless this interpolation is useful to model the strain rate when the data are sparse.

To relate the deformation rate to seismicity, independently from the style of deformation (different in extensional, contractional and strike-slip tectonic settings), we have considered the 2D second invariant of the strain rate tensor, defined as the scalar $\mathrm{SR} = \sqrt{(\dot{\varepsilon}_{11}^2 + \dot{\varepsilon}_{22}^2 + 2 \cdot \dot{\varepsilon}_{12}^2)}$ accounting for all the deformation tensor components (Kreemer et al., 2003), so that it represents the total strain rate (SR).

We have mapped the SR of the Italian area on a regular grid of $0.1^\circ \times 0.1^\circ$ by The Generic Mapping Tools (GMT, Wessel and Smith, 1998), as shown in Fig. 1A. The deformation rates are not uniformly distributed, they range from zero to $\sim 90 \times 10^{-9}\ \mathrm{yr}^{-1}$ with maximum values along the Apennine belt, around the Messina Strait, the NE Alpine sector and Dinarides. Along the whole Apennine chain the ongoing extension is clearly evident from the velocity field expressed with respect to the Eurasian plate (Devoti et al., 2011), so that it represents a major contributor to the deformation rate along the Italian peninsula (Fig. 1A). The average uncertainty of the deformation rates is about $10 \times 10^{-9}\ \mathrm{yr}^{-1}$ (Fig. 1B), reaching higher level in few zones; note the local high rate detected in NW Italy (Fig. 1A) appears not significant (Fig. 1B).

Although the grid does not allow for a resolution at fault level, the observed strain rates suggest that some sectors of the Apennines domain could be approaching the end of the interseismic phase of the earthquake cycle.

3. Recent seismicity of Italy and SR

The Italian area is characterised by moderate seismicity (Chiarabba et al., 2005) distributed in a continuous belt of upper crustal seismicity along the Apennines, a contiguous region of deeper crustal events east of the upper crustal seismic belt and sub-crustal earthquakes beneath the northern Apennines, the Calabrian arc, and sporadically in the Alps.

Focal mechanism solutions (Pondrelli et al., 2011) show predominant normal faulting mechanisms all along the Apennines most elevated ridges, while thrust faulting is observed in low topography areas such as the southern Alps front and in the external part of the Apennine accretionary prism (Carminati et al., 2004).

The Italian area has a good record of historical (e.g., Locati et al., 2011; Rovida et al., 2011) and instrumental seismicity and its main

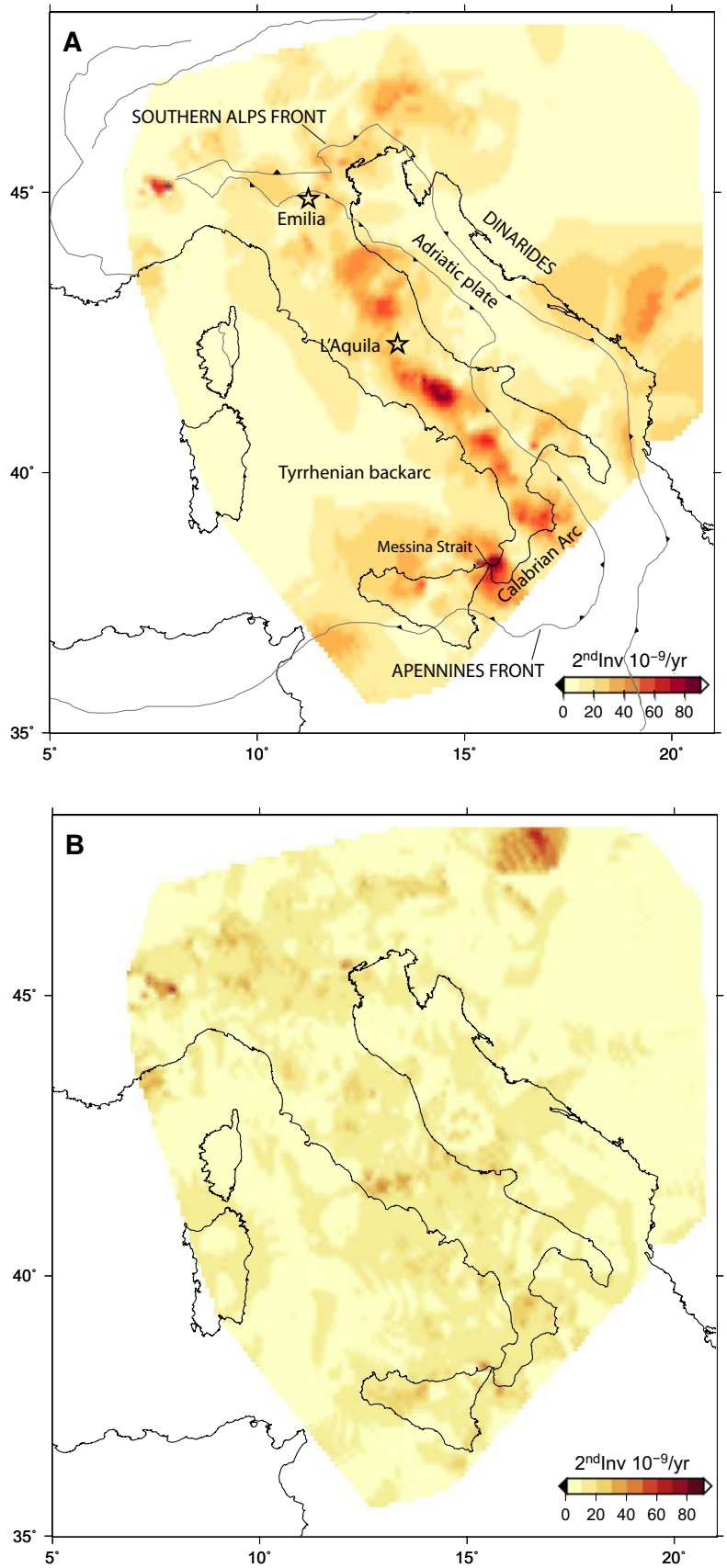

Fig. 1. Geodetic strain rate and uncertainty. (A) Map of the second invariant of 2D strain rate tensor (SR) estimated from the 2D velocity field of the Italian area (Devoti et al., 2011) and obtained after the interpolation and smoothing techniques developed by Shen et al. (1996). The gray line delimits the "undeformed" part of the Adriatic microplate and represents the active fronts of deformation. The Adriatic microplate goes in subduction along the Apennines and Dinarides and overrides the Eurasian plate along the Alps. Stars indicate the locations of the recent 6 April 2009 L'Aquila and 20 May 2012 Emilia events. (B) Map of the SR uncertainty.

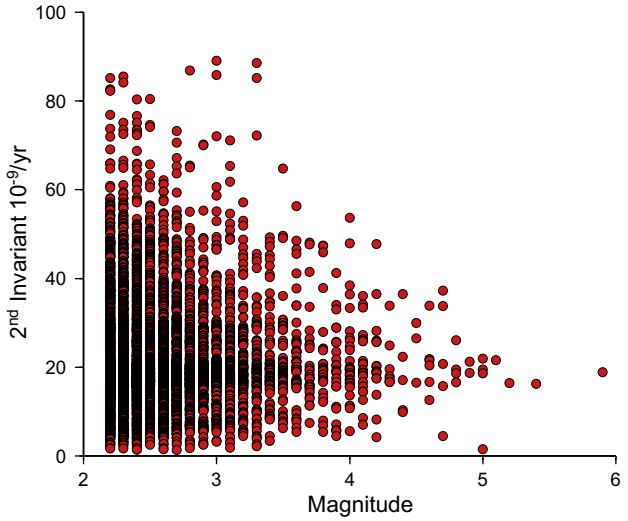

Fig. 2. Geodetic strain rate and earthquake size. Low magnitude events occur in all the SR classes, larger magnitudes occur toward lower SR classes, database of 6380 events with $M_L \geqslant 2.2$ (http://iside.rm.ingv.it) and SR values interpolated at the epicentre coordinates.

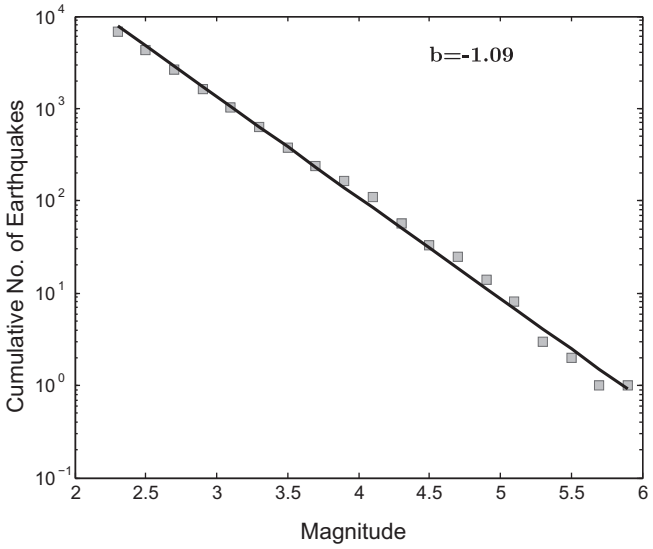

Fig. 3. Gutenberg–Richter distribution. Log-scaled cumulative number of seismic events (#6380, $M_L \geqslant 2.2$) in classes of $\Delta M = 0.2$. The straight line represents the Gutenberg–Richter relationship with slope given by the *b*-value (Gutenberg and Richter, 1954).

seismogenic trends are quite well established (Basili et al., 2008), however some earthquake sequences occur in largely unexpected areas (Valensise et al., 2004) due to the presence of blind or buried active faults, thus preventing dedicated monitoring.

We have considered all the crustal seismic events localised by the Italian seismic network of INGV from 1 January 2007 to 31 December 2011 (http://iside.rm.ingv.it) in a region larger than the Italian area, delimited by longitudes 6–21° E and latitudes 35–48° N. The aim of selecting a limited time interval is to manage a sort of snapshot of the recent seismicity to be related to the 'instantaneous' deformation field, i.e. not affected by non-linear processes like co- and postseismic effects. The ISIDE database of INGV releases local magnitudes (M_L) reaching a completeness level for $M_L \geqslant 1.6$ in most of the seismogenic areas. The primary dataset consists of 7116 events with $2.2 \leqslant M_L \leqslant 5.9$, localised within 40 km depths.

We have interpolated the value of the SR at the coordinates of each seismic event using GMT (Wessel and Smith, 1998), so that the magnitude of each event is associated with the value of deformation rate at epicentre. Events occurred in cells where the SR is undefined, i.e. falling outside the GPS network limits, have been excluded from our analysis, so that the seismic dataset reduces to 6830 events.

The plot of SR vs magnitude shows a peculiar behaviour (Fig. 2), evidence of a non-random relationship: low magnitude earthquakes occur at all SR values, while larger magnitudes occur at lower SR only.

4. Bayesian probability relationship between magnitude and SR

The clear pattern evidenced in Fig. 2 pushed us to look for the probability of magnitude occurrence in a given SR interval; we derived the analytical expression of the corresponding probability density function following a Bayesian approach (Koch, 1990; Sansò and de Lacy, 2006), in which the a priori magnitude distribution follows the GR law (Fig. 3). Such distribution is commonly described by a power law in which its slope is a critical parameter in seismology that describes the magnitude distribution of events. A high *b*-value indicates a relatively larger proportion of smaller events, and vice versa. A catalogue of events with *b*-value ~1 indicates a balanced proportion between the magnitudes (Gutenberg and Richter, 1954).

We found the simple form (see the following sub-sections) for the probability density that an earthquake of a given magnitude *M* occurs in a given SR class (represented in the formulas by *S*)

$$f(M|S) = \frac{1}{\mu(M|S)} \cdot e^{-\frac{M}{\mu(M|S)}} \tag{1}$$

where $\mu(M|S)$ is the normalised average magnitude *M* of earthquakes occurred in a given class of SR.

4.1. Method fundamentals

The Bayesian approach is based on the Bayes theorem and gives the relationship between the probabilities of two random events *E1* and *E2*, *P*(*E1*) and *P*(*E2*), and the conditional probabilities of *E1* given *E2* and *E2* given *E1*, *P*(*E1*|*E2*) and *P*(*E2*|*E1*), allowing to account for all the available a priori information about the two events (Koch, 1990).

In our case *E1* and *E2* are, respectively the strain rate *S* and the magnitude *M*. According to the Bayesian approach, the probability density *f*(*M*|*S*) of the magnitude *M* given the strain rate *S*, reads

$$f(M|S) = \frac{f(S|M) \cdot f(M)}{f(S)} \tag{2}$$

in which $f(S) = \int f(S|M) f(M) dM$ is the normalisation constant fulfilling the condition $\int f(M|S) dM = 1$.

4.2. A priori magnitude probability density function

The a priori probability density function *f*(*M*) comes from the GR law $\log N = a - b \cdot M$, where *N* is the cumulative number of earthquakes of magnitude *M* or greater, *a* is the earthquake productivity of a volume, and *b* is the relative size coefficient (Wiemer and Wyss, 2002).

$$f(M) = A \cdot e^{-B \cdot M} \tag{3}$$

with $A = \frac{10^a}{N_{\text{tot}}}$ and $B = b \cdot \ln 10$, in which *a* and *b* are the GR's coefficients.

4.3. A priori conditional probability density function of SR

We hypothesise that the probability density function $f(S|M)$ can be written as

$$f(S|M) = h \cdot S^{l \cdot M} \cdot e^{-k \cdot M \cdot S} \quad (4)$$

where h, l and k are parameters defining the family of curves describing the probability density function of S given M.

Taking into account that the histograms of S show a persistent maximum at $S = S_{max}$ independent from M (Fig. 4), imposing the condition $f'(S|M) = 0$, then $S_{max} = \frac{1}{k \cdot M} = \frac{1}{c}$, we can write (4) as

$$f(S|M) = h \cdot S^{l \cdot M} \cdot e^{-c \cdot S} \quad (5)$$

which behaves like a χ^2 distribution with n degrees of freedom

$$f(x) = \frac{1}{2^{\frac{n}{2}}\Gamma\left(\frac{n}{2}\right)} \cdot x^{\frac{n}{2}-1} \cdot e^{-\frac{x}{2}}$$

imposing $c = \frac{1}{2}$, $l \cdot M = \frac{n}{2} - 1$ (then $n = 2(l \cdot M + 1)$, $h = \frac{1}{2^{\frac{n}{2}}\Gamma\left(\frac{n}{2}\right)}$.

Taking into account the normalisation condition $\int_0^\infty f(S|M)ds = 1$ we obtain

$$f(S|M) = \frac{1}{2^{(l \cdot M+1)}\Gamma(l \cdot M + 1)} \cdot S^{l \cdot M} \cdot e^{-\frac{S}{2}} = \chi^2_{2(l \cdot M+1)} \quad (6)$$

with mean $\mu(S|M) = \int_0^\infty S \cdot f(S|M)dS = 2(l \cdot M + 1)$ and hence $l = \frac{\mu(S|M)-2}{2M}$.

4.4. SR probability density function

Therefore, considering (3) and (6), the SR probability density function results

$$f(S) = \int_\infty^0 f(S|M) \cdot f(M)dM = \frac{hAe^{-c \cdot S}}{B - l \cdot lnS} \quad (7)$$

in which A and B depend on the GR coefficients, as in (3).

4.5. Bayesian magnitude conditional probability density function

In the end, substituting into (2) each term coming from (3), (4), and (7)

$$f(M|S) = (B - l \cdot lnS) \cdot S^{l \cdot M} \cdot e^{-B \cdot M} \quad (8)$$

and imposing the normalisation condition $\int_0^\infty f(M|S)dM = 1$ taking into account that the mean is

$$\mu(M|S) = \int_\infty^0 M \cdot f(M|S)dM = \frac{1}{B - l \cdot lnS} \quad (9)$$

we obtain the family of curves with exponential decay (1), simply calibrated by the average normalised magnitude occurred in each SR class $\mu(M|S)$

$$f(M|S) = \frac{1}{\mu(M|S)} \cdot e^{-\frac{M}{\mu(M|S)}} \quad (1)$$

5. Discussion

To compare the analytical family of curves (1) with the observed values, we have considered only events with $3.0 \leqslant M \leqslant 6.0$ (#1029, Fig. 5), to eliminate the noisy part of the SR vs magnitude distribution at low magnitude values (evident in Fig. 2). Then, we calculated the probability density $f_{obs}(M|S)$ in the form of (1), from the histograms of M in classes of SR (Fig. 6), where (according to histogram definition) the height of each class is equal to the frequency density of the interval, i.e. the frequency divided by the width of the magnitude interval (being $\Delta M = 0.2$). Then, we compared the modelled probability density (1) and the observed frequency in four SR classes (0–20, 20–40, 40–60, 60–85) $\times 10^{-9}$ yr^{-1}, showing the results in Fig. 7. We normalised the magnitude M in the interval $0 \leqslant Mn \leqslant 1$, in order to make our analysis more general and independent from the chosen set of events, which however was recognised well distributed with respect the Gutemberg–Richter criterion (b-value ~1 in the GR law). Each panel of Fig. 7 shows the log-scaled probability density both vs the normalised magnitude ($0 \leqslant Mn \leqslant 1$, horizontal axis, bottom), and the magnitude ($3.0 \leqslant M \leqslant 6.0$, horizontal axis, top) for each class of S. In Fig. 7, the straight lines are the modelled functions obtained from (1), the symbols are the observed values (gray tones for the first two SR classes, red tones for the others).

The μ-value, i.e. the inverse of each slope, is the statistical average of M in each SR class and can be considered a critical parameter proportional to the earthquake size probability in a given a class of

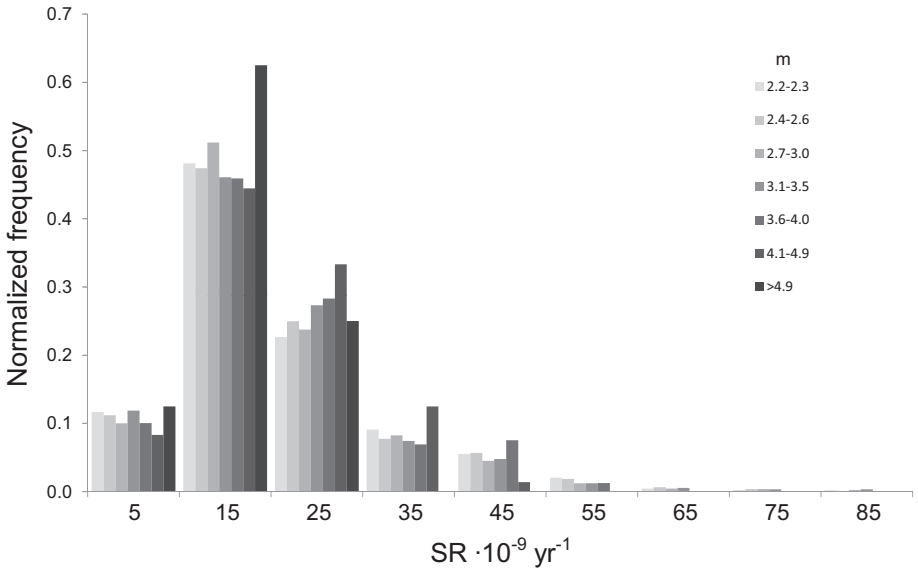

Fig. 4. Probability density of SR. Histograms of SR in magnitude classes, the maximum number of events occur persistently in the class (10–20) $\times 10^{-9}$ yr^{-1}, independently from magnitude values.

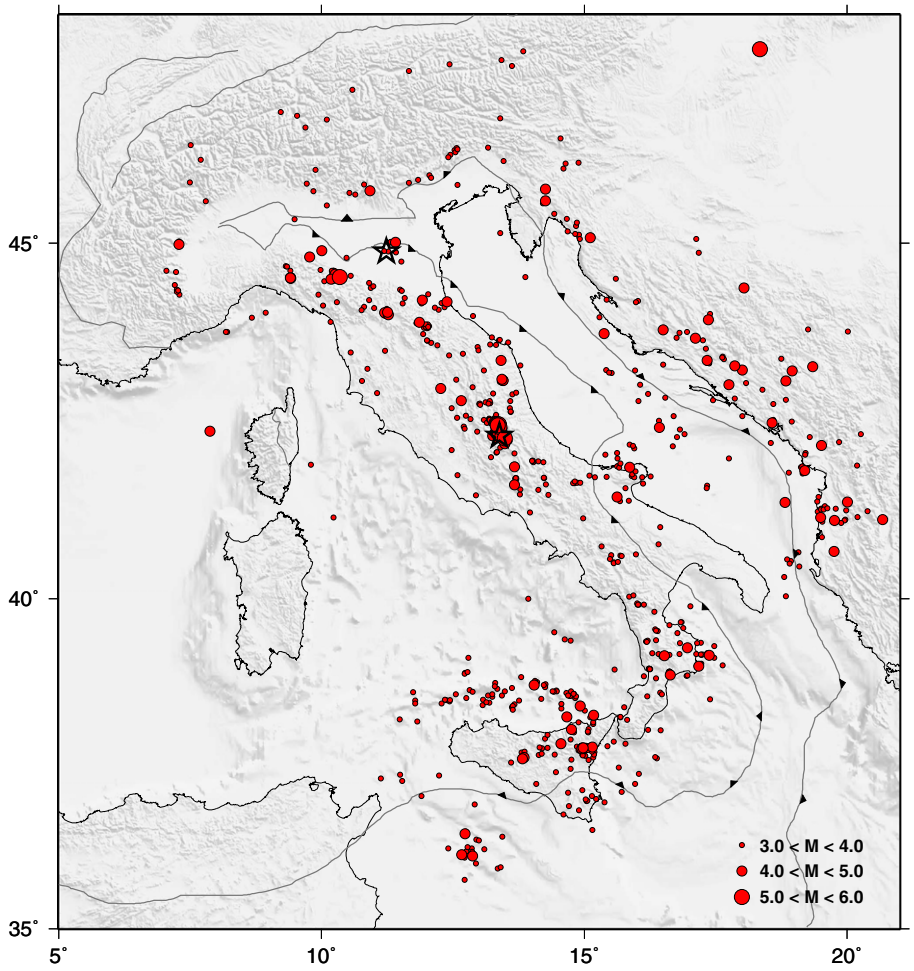

Fig. 5. Seismicity of the Italian area. Earthquakes with $M_L \geqslant 3.0$ (#1029) occurred from 1 January 2007 to 31 December 2011 within 40 km depth. Circles are proportional to magnitude values. At each earthquake epicentre corresponds one SR value obtained after interpolation (Wessel and Smith, 1998) from the SR-grid (Fig. 1A and B). Stars indicate the locations of the recent 6 April 2009 L'Aquila and 20 May 2012 Emilia events.

SR. Inversely to the interpretation of *b*-value, according to which a high *b*-value indicates a relatively larger proportion of small events, and vice versa (e.g., Wiemer and Wyss, 2002), high μ-value indicates a relatively higher probability of large events.

In fact, the probability to have an earthquake with $M \geqslant 4.0$, that is $Mn \geqslant 0.33$ (the integral of $f(M|S)$ for $M \geqslant 4.0$) is ~9.1% in the 0–20 SR class ($\mu = 0.14$), ~10.3% with SR 20–40 ($\mu = 0.15$), ~7.6% with SR 40–60 ($\mu = 0.13$) and ~0.5% with SR 60–85 ($\mu = 0.6$).

Therefore, according to the aforementioned observations, a significant earthquake has higher probability to occur in areas characterised by low SR during the interseismic period. Thus on average, in tectonically active areas, low SR regions appear to behave as being in a late stage of the seismic cycle, where the accumulated stress reaches a maximum and the faults are proximal to failure.

A retrospective analysis can be made on the recent significant seismic events occurred in Italy at L'Aquila (6 April 2009, 13.38E 42.34 N, $M_L = 5.9$, central Apennines, extensional mechanism) and in Emilia region (20 May 2012, 11.23E 44.89 N, $M_L = 5.9$, northern Apeninnes, thrust mechanism). Both the events occurred in areas of low SR, near areas of higher SR, thus representing two case history of faults activated at the end of the seismic cycle.

The overall deformation rate (SR) measured by GPS in the epicentral area during the preseismic period is $\sim 19 \times 10^{-9}\ \mathrm{yr}^{-1}$ around L'Aquila and $\sim 14 \times 10^{-9}\ \mathrm{yr}^{-1}$ in Emilia, both just over the significance level.

Since the two areas are characterised by low preseismic strain rates, both fall in the first SR class of our analysis (Fig. 7, first panel). The probability to have an earthquake with $M \geqslant 4.0$ results in 9.1% which turn out to be SR zones with higher occurrence probability.

6. Conclusions

The analysis of the SR and its variation through time in a tectonically active area can be a powerful tool in predicting the location and the expected magnitude of future earthquakes. High SR areas can be interpreted as regions where both the upper and the lower crust are creeping, or alternatively where tectonic loading is more effective (early stage in seismic cycle), so that low magnitude earthquakes are expected. Vice versa lower strain rates suggest the presence of locked faults in a later stage in seismic cycle and then the expected magnitudes could be higher.

Therefore we treated the regional SR as a stochastic variable, studying the stochastic dependence between seismic activity and local deformation rate in order to understand whether an area is in the proximity of a seismic event.

We have shown how a simple exponential decreasing function provides the probability density for an event of a given magnitude to fall within a given SR interval, along the Italian peninsula. It is expected that the derived probability density function (1) does

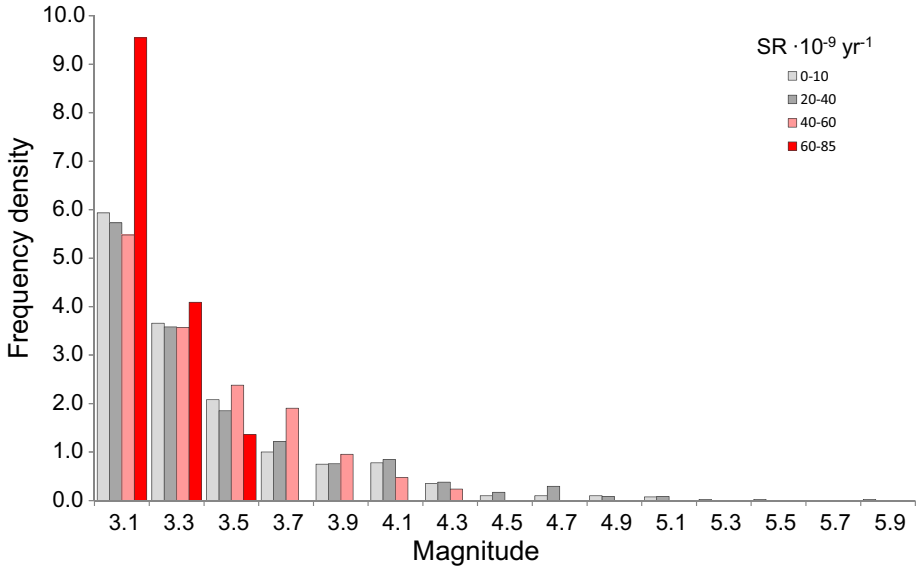

Fig. 6. Relative frequencies of magnitudes in classes of SR. The height of each class is equal to the frequency density of the interval, i.e. the frequency divided by the width of the interval ($\Delta M = 0.2$). We consider here 1029 events with $M_L \geqslant 3.0$; gray tones: $(0–20, 20–40) \times 10^{-9}$ yr^{-1}, red tones $(40–60, 60–85) \times 10^{-9}$ yr^{-1}. (For interpretation of the references to colour in this figure legend, the reader is referred to the web version of this article.)

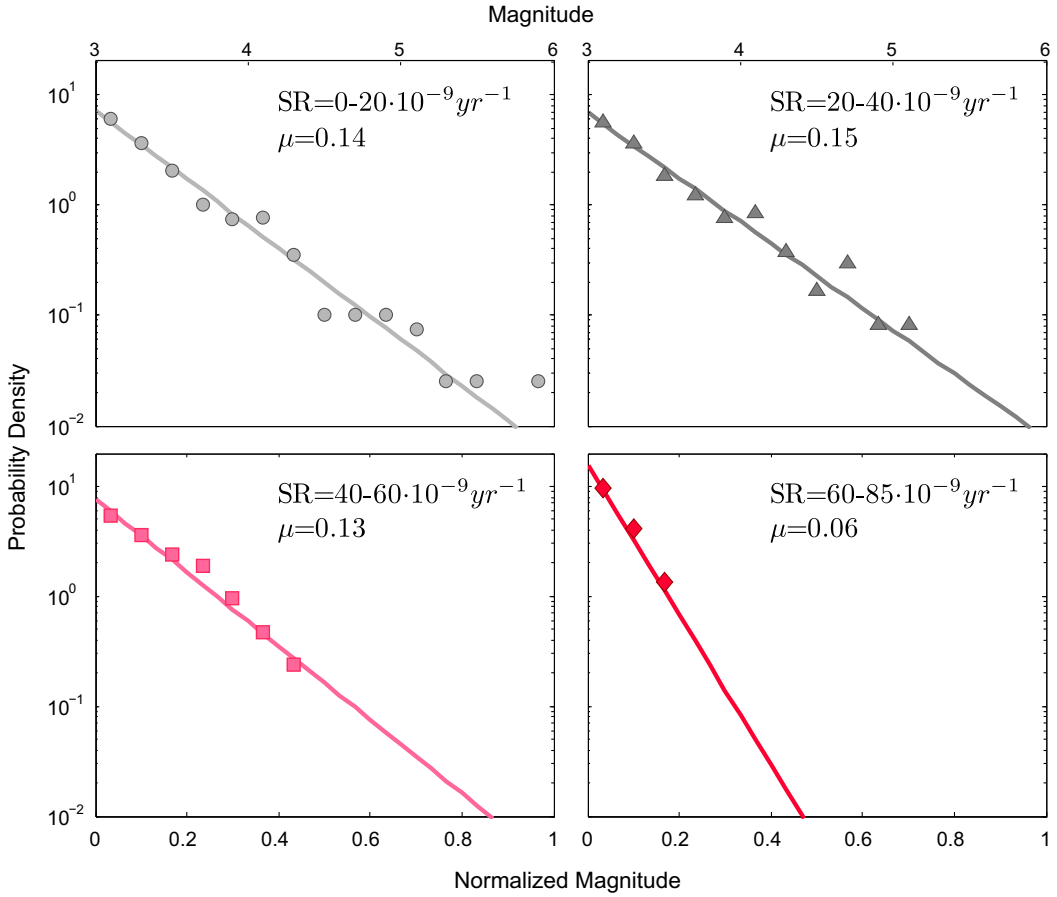

Fig. 7. Log-scaled probability density vs normalised magnitude. Panels refer to different classes of SR. We normalised the magnitudes $3.0 \leqslant M \leqslant 6.0$ in the interval $0 \leqslant Mn \leqslant 1$, so each ΔMn = 0.2 corresponds to $\Delta M = 0.6$. The straight lines are the modelled functions (1), the symbols are the observed values (gray tones the first two SR classes, red tones the others). The μ-value, i.e. the inverse of each slope, is the statistical average of M in each SR class. (For interpretation of the references to colour in this figure legend, the reader is referred to the web version of this article.)

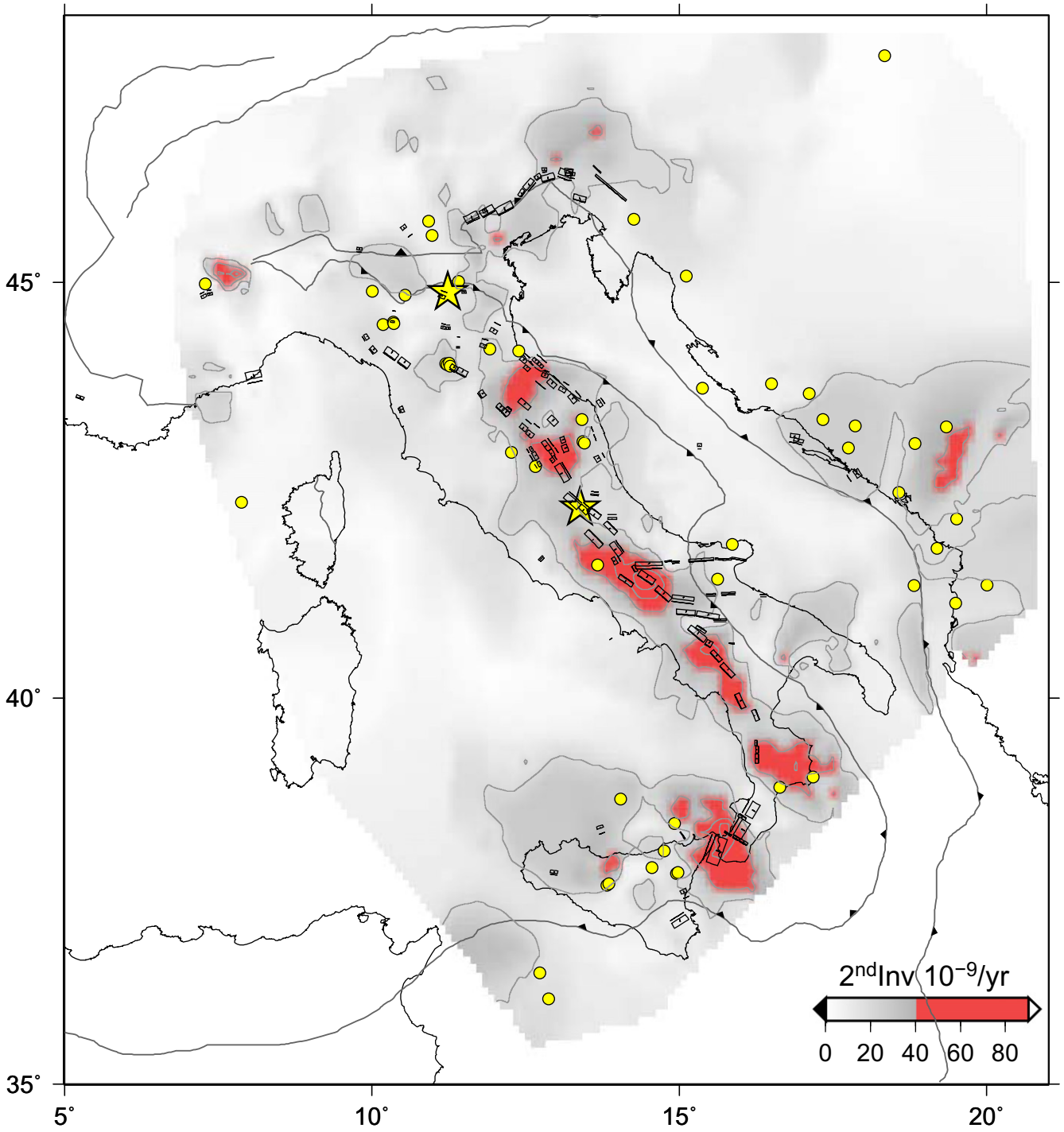

Fig. 8. Earthquakes with $M > 4.0$ and SR map. SR of Fig. 1A mapped with a bicoloured palette (gray areas: two lower classes (0–40) $\times 10^{-9}$ yr^{-1}, red areas: the higher classes (40–85) $\times 10^{-9}$ yr^{-1}). Regardless the tectonic setting (extension, compression, strike-slip), all but one of events (yellow circles) are located in gray areas. The black boxes are the individual seismogenetic sources reported in the DISS database (Basili et al., 2008). Stars indicate the locations of the recent 6 April 2009 L'Aquila and 20 May 2012 Emilia events. From this map we could infer that the red areas should not experience large earthquakes in the next future. (For interpretation of the references to colour in this figure legend, the reader is referred to the web version of this article.)

not depend critically on the completeness of the earthquake catalogue at all magnitudes, since our calibration dataset has *b*-value ~1 (Fig. 3), so that it can be used also with higher magnitudes; in this last respect, historical catalogues show that the maximum magnitude ever occurred in Italy was $M = 7.4$ in south-eastern Sicily on 1693 (e.g., Locati et al., 2011; Rovida et al., 2011). Even if in our opinion an increase of the magnitude values should not affect the analytical form of the probability density (1), future re-calibrations of the distributions performed over other data sets are desirable, even with simulated catalogues.

We noticed that larger earthquakes occur with higher probability in areas of lower SR, in particular events with $M > 4.0$ occur mainly in areas where SR $\leqslant 40 \times 10^{-9}$ yr^{-1} (Figs. 2 and 7). From our analysis it is reasonable to consider this SR value as a bound

separating areas characterised by significant seismic activity from areas affected by background seismicity, in the considered time interval. As conveniently represented in Fig. 8 by the bicoloured palette (gray, low SR; red, higher SR), the whole area with low SR is wider than the area with higher SR. In terms of seismic hazard assessment (e.g., Zuccolo et al., 2011), this fact implies a larger spatial uncertainty of occurrence for larger earthquakes (gray area). On the contrary, we can observe that the red areas have low probability to generate earthquakes with $M > 4.0$, but unfortunately they constitute only a small region. Therefore, for a more significant contribution to hazard assessment, it is worth to underline that the map of the SR (Figs. 1 and 8) must clearly be tied with the map of the active faults of the study area, since low SR can be found also in regions where no present tectonics is expected. In this respect, the analysis must be combined with the present geological, geophysical and space geodesy data of the study area indicating the active faults, regardless they reach the surface, or are rather buried blind faults.

Overall, in the next future, the proposed approach could really represent an effective tool in order to determine areas where higher seismic risk is concentrated, starting from an accurate mapping of the actual SR analysis, possibly coupled with geological and geophysical information which can be introduced into the probability density function as well (e.g., Borghi et al., 2009; Mignan and Di Giovambattista, 2008).

Acknowledgements

We wish to acknowledge the effort of all the people working on regional and worldwide GPS permanent networks and database maintenance (ASI, EUREF, INGV, INOGS, SOPAC and many other institutions, universities and agencies). The authors gratefully acknowledge V. Kossobokov and an anonymous referee for the constructive review and the Associate Editor M. Jellinek for his advices and courtesy. We are grateful to S. Barba, E. Carminati, G. Panza, A. Peresan for fruitful discussions.

References

Anzidei, M., Boschi, E., Cannelli, V., Devoti, R., Esposito, A., Galvani, A., Melini, D., Pietrantonio, G., Riguzzi, F., Sepe, V., Serpelloni, E., 2009. Coseismic deformation of the destructive April 6, 2009 L'Aquila earthquake (central Italy) from GPS data. Geophys. Res. Lett. 36, L17307. http://dx.doi.org/10.1029/2009GL039145.

Avallone, A., Selvaggi, G., D'Anastasio, E., D'Agostino, N., Pietrantonio, G., Riguzzi, F., Serpelloni, E., Anzidei, M., Casula, G., Cecere, G., D'Ambrosio, C., DeMartino, P., Devoti, R., Falco, L., Mattia, M., Rossi, M., Obrizzo, F., Tammaro, U., Zarrilli, L., 2010. The RING network: improvement of a GPS velocity field in the central Mediterranean. Ann. Geophys. 53 (2), 39–54.

Basili, R., Valensise, G., Vannoli, P., Burrato, P., Fracassi, U., Mariano, S., Tibert, M.M., Boschi, E., 2008. The Database of Individual Seismogenic Sources (DISS), version 3: summarizing 20 years of research on Italy's earthquake geology. Tectonophysics 453, 20–43.

Bird, P., Kreemer, C., Holt, W.E., 2010. A long-term forecast of shallow seismicity based on the Global Strain Rate Map. Seismol. Res. Lett. 81 (2), 184–194. http://dx.doi.org/10.1785/gssrl.81.2.184.

Blewitt, G., Lavallée, D., 2002. Effect of annual signals on geodetic velocity. J. Geophys. Res. 107 (B7). http://dx.doi.org/10.1029/2001JB000570.

Borghi, A., Aoudia, A., Riva, R.E.M., Barzaghi, R., 2009. GPS monitoring and earthquake prediction: a success story towards a useful integration. Tectonophysics 465 (1–4), 177–189.

Caporali, A., Barba, S., Carafa, M.M.C., Devoti, R., Pietrantonio, G., Riguzzi, F., 2011. Static stress drop as determined from geodetic strain rates and statistical seismicity. J. Geophys. Res. 116, B02410.

Carminati, E., Doglioni, C., Barba, S., 2004. Reverse migration of seismicity on thrusts and normal faults. Earth Sci. Rev. 65, 195–222.

Cavalié, O., Lasserre, C., Doin, M.-P., Peltzer, G., Sun, J., Xud, X., Shen, Z.-K., 2008. Measurement of interseismic strain across the Haiyuan fault (Gansu, China), by InSAR. Earth Planet. Sci. Lett. 275, 246–257.

Chiarabba, C., Jovane, L., Di Stefano, R., 2005. A new view of Italian seismicity using 20 years of instrumental recordings. Tectonophysics 395, 251–268.

Dal Piaz, G.V., 2010. The Italian Alps: a journey across two centuries of Alpine geology. J. Virtual Explorer 36, ISSN 1441-8142.

Devoti, R., Riguzzi, F., Cuffaro, M., Doglioni, C., 2008. New GPS constraints on the kinematics of the Apennines subduction. Earth Planet. Sci. Lett. 273, 163–174.

Devoti, R., Esposito, A., Pietrantonio, G., Pisani, A.R., Riguzzi, F., 2011. Evidence of large scale deformation patterns from GPS data in the Italian subduction boundary. Earth Planet. Sci. Lett. 311, 230–241.

Devoti, R., Anderlini, L., Anzidei, M., Esposito, A., Galvani, A., Pietrantonio, G., Pisani, A.R., Riguzzi, F., Sepe, V., Serpelloni, E., in press. The coseismic and postseismic deformation of the L'Aquila, 2009 earthquake from repeated GPS measurements. Ital. J. Geosci. 131 (3). http://dx.doi.org/10.3301/IJG.2012.15.

Dixon, T., Decaix, J., Farina, F., Furlong, K., Malservisi, R., Bennett, R., Suarez-Vida, L.F., Fletcher, J., Lee, J., 2002. Seismic cycle and rheological effects on estimation of present-day slip rates for the Agua Blanca and San Miguel-Vallecitos faults, northern Baja California, Mexico. J. Geophys. Res. 107 (B10), 2226. http://dx.doi.org/10.1029/2000JB000099.

Doglioni, C., 1991. A proposal of kinematic modelling for W-dipping subductions – possible applications to the Tyrrhenian–Apennines system. Terra Nova 3 (4), 423–434.

Doglioni, C., Barba, S., Carminati, E., Riguzzi, F., 2011. Role of the brittle–ductile transition on fault activation. Phys. Earth Planet. Inter. 184, 160–171.

Fialko, Y., 2006. Interseismic strain accumulation and the earthquake potential on the southern San Andreas fault system. Nature 441, 968–971.

Gutenberg, B., Richter, C.F., 1954. Seismicity of the Earth and Associated Phenomena, second ed. Princeton University Press, Princeton, NJ.

Hammond, W.C., Kreemer, C., Blewitt, G., Plag, H.P., 2010. Effect of viscoelastic postseismic relaxation on estimates of interseismic crustal strain accumulation at Yucca Mountain, Nevada. Geophys. Res. Lett. 37, L06307.

Koch, K.R., 1990. Bayesian inference with geodetic data. Lecture Notes in Earth Sciences, Vol. 31. Springer.

Kreemer, C., Holt, W.E., Haines, A.J., 2003. An integrated global model of present-day plate motions and plate boundary deformation. Geophys. J. Int. 154, 8–34. http://dx.doi.org/10.1046/j.1365-246X.2003.01917.x.

Liu, M., Yang, Y., Stein, S., Zhu, Y., Engeln, J., 2000. Crustal shortening in the Andes: why do GPS rates differ from geological rates? Geophys. Res. Lett. 27 (18), 3005–3008.

Locati, M., Camassi, R., Stucchi, M., 2011. DBMI11, the 2011 version of the Italian Macroseismic Database. Milano, Bologna. <http://emidius.mi.ingv.it/DBMI11>.

Loveless, J.P., Meade, B.J., 2011. Spatial correlation of interseismic coupling and coseismic rupture extent of the 2011 M(W) = 9.0 Tohoku-oki earthquake. Geophys. Res. Lett. 38, L17306. http://dx.doi.org/10.1029/2011GL048561.

Lundgren, P., Hetland, E.A., Liu, Z., Fielding, E.J., 2009. Southern San Andreas-San Jacinto fault system slip rates estimated from earthquake cycle models constrained by GPS and interferometric synthetic aperture radar observations. J. Geophys. Res. 114, B02403. http://dx.doi.org/10.1029/2008JB005996.

Mignan, A., Di Giovambattista, R., 2008. Relationship between accelerating seismicity and quiescence, two precursors to large earthquakes. Geophys. Res. Lett. 35, L15306. http://dx.doi.org/10.1029/2008GL035024.

Pondrelli, S., Salimbeni, S., Morelli, A., Ekström, G., Postpischl, L., Vannucci, G., Boschi, E., 2011. European-Mediterranean Regional Centroid Moment Tensor Catalog: solutions for 2005–2008. Phys. Earth Planet. Int. 185 (3–4), 74–81.

Rovida, A., Camassi, R., Gasperini, P., Stucchi, M. (Eds.), 2011. CPTI11, the 2011 version of the Parametric Catalogue of Italian Earthquakes. Milano, Bologna. <http://emidius.mi.ingv.it/CPTI>.

Sansò, F., de Lacy, M.C., 2006. The Bayesian approach applied to significant deformation identification. In: Geodetic Deformation Monitoring: From Geophysical to Engineering Roles, vol. 131, International Association of Geodesy Symposia, Jaen, March 2005, Springer-Verlag, Berlin, Heidelberg, pp. 200–208.

Savage, J.C., Prescott, W.H., 1978. Asthenosphere readjustment and the earthquake cycle. J. Geophys. Res. 83, 3369–3376.

Shen, Z.K., Jackson, D.D., Ge, B.X., 1996. Crustal deformation across and beyond the Los Angeles basin from geodetic measurements. J. Geophys. Res. 101, 27957–27980.

Shen, Z.K., Jackson, D.D., Kagan, Y.Y., 2007. Implications of geodetic strain rate for future earthquakes, with a five-year forecast of M5 earthquakes in Southern California. Seismol. Res. Lett. 78, 116–120.

Stein, S., 1992. Seismic gaps and grizzly bears. Nature 356, 387–388.

Valensise, G., Pantosti, D., Basili, R., 2004. Seismology and Tectonic Setting of the 2002 Molise, Italy. Earthquake Spectra 20, S23–S37.

Wessel, P., Smith, W.H.F., 1998. New, improved version of Generic Mapping Tools released. EOS Trans. Am. Geophys. U. 79 (47), 579.

Wiemer, S., Wyss, M., 2002. Mapping spatial variability of the frequency–magnitude distribution of earthquakes. Adv. Geophys. 45, 259–302.

Zuccolo, E., Vaccari, F., Peresan, A., Panza, G.F., 2011. Neo-deterministic and probabilistic seismic hazard assessments: a comparison over the Italian Territory. Pure Appl. Geophys. 168, 69–83.